Journal of Sound and Vibration 329 (2010) 4772–4784

Contents lists available at ScienceDirect

Journal of Sound and Vibration

journal homepage: www.elsevier.com/locate/jsvi

Hysteretic damping in rotordynamics: An equivalent formulation

Giancarlo Genta, Nicola Amati *

Politecnico di Torino, Department of Mechanics, Corso Duca degli Abruzzi 24, 10029 Torino, Italy

ARTICLE INFO

Article history:
Received 1 September 2009
Received in revised form
20 April 2010
Accepted 21 April 2010
Handling Editor: S. Ilanko
Available online 18 June 2010

ABSTRACT

The hysteretic damping model cannot be applied to time domain dynamic simulations: this is a well-known feature that has been discussed in the literature since the time when analog computers were widespread. The constant equivalent damping often introduced to overcome this problem is also discussed, and its limitations are stated, in particular those linked with its application in rotordynamics to simulate rotating damping. An alternative model based on the nonviscous damping (NVD) model, but with a limited number of additional degrees of freedom, is proposed, and the relevant equations are derived. Some examples show applications to the rotordynamics field.

1. Introduction

The damping properties of structures are usually modeled by introducing a term that is linear with the velocity into the equation of motion. This model is usually referred to as viscous damping. When dealing with rotating structures or rotors this approach leads to two separate terms, one proportional to the deformation velocity and one to the rotational velocity and the displacements. The latter causes a circulatory matrix to be present in the linearized equation of motion and has a destabilizing effect [1].

An alternative is to use the so-called structural or hysteretic damping model [2]. It is essentially based on the observation that the energy losses in engineering materials undergoing cyclic loading are proportional to the square of the amplitude and almost independent of frequency, at least within a wide frequency range.

There has been much discussion in the last 60 years on the validity of such assumptions, but the fact remains that the dependence on the square of the amplitude allows for the introduction of linear models, and the independency of frequency (which amounts to saying that the phase lag between stresses and strains is essentially constant and independent of the frequency) allows for the definition of a constant complex stiffness, or complex Young's modulus when working at the level of material properties. Clearly, the last assumption cannot hold when the frequency of the hysteresis cycle tends to zero.

The hysteretic damping model is usually applied by defining a complex elastic modulus, if at the level of the characteristics of the material, or a complex stiffness, if at the level of the mechanical element. Under the assumptions above, the real and imaginary parts of the former (usually referred to as E' and E'') and their ratio, the loss factor

$$\eta = \frac{E''}{E'},$$

are considered as constants and are characteristics of the material.

* Corresponding author. Fax: +39 011 564 6999.
E-mail addresses: giancarlo.genta@polito.it (G. Genta), nicola.amati@polito.it (N. Amati).
URL: http://www.giancarlogenta.it (G. Genta).

0022-460X/$ - see front matter © 2010 Elsevier Ltd. All rights reserved.
doi:10.1016/j.jsv.2010.04.036

Nomenclature

c	viscous damping coefficient
c_{eq}	equivalent viscous damping
$\mathbf{C}$	damping matrix
$\overline{\mathbf{C}}$	modal damping matrix
E	Young's modulus
f	generalized force
$\mathbf{G}$	gyroscopic matrix
$\overline{\mathbf{G}}$	modal gyroscopic matrix
i	imaginary unit
k	stiffness
$\mathbf{K}$	stiffness matrix
$\overline{\mathbf{K}}$	modal stiffness matrix
m	mass
$\mathbf{M}$	mass matrix
$\overline{\mathbf{M}}$	modal mass matrix
n	number of spring–damper branches
$\mathbf{r}$	vector of the complex coordinates
t	time
$\mathbf{x}$	vector of the generalized coordinates
η	loss factor
$\boldsymbol{\eta}$	modal coordinates
σ	decay rate
Φ	eigenvector matrix
ω	circular frequency, whirl speed
Ω	spin speed

Subscripts

eq	equivalent
n	nonrotating
r	rotating

It is well known that the hysteretic damping model can be applied only to systems with harmonic motion [3], which means that it can be introduced into equations of motion referred to the frequency domain but not to the time domain [4]. The impossibility of using the hysteretic damping model in time domain formulations is a severe limitation, in particular because numerical simulation, based on the numerical integration in time of the equations of motion, is now a basic tool in the dynamic analysis of systems of all types.

Another critical issue is that hysteretic damping may overestimate the damping properties of materials when the vibration frequency is very low. Actually, if the vibration frequency tends to zero, it yields inconsistent results, which may not be an issue in structural dynamics, but it is in rotordynamics because synchronous whirling is seen by the material constituting the rotor as a vibration at vanishing frequency. This limitation has not prevented the use of the hysteretic damping model in rotordynamics [5,6], but it has caused misunderstanding and incorrect interpretations [7].

The issue of looking for a model equivalent to hysteretic damping, but suitable for time domain formulations, was particularly felt in the 1950s and 1960s, in connection with the use of analog computers. Analog computers could be used only to study time-domain problems, and thus the usual hysteretic damping model could not be implemented on them.

Biot [8] and Caughey [9] showed that the model the former called 'Voigt model of viscoelasticity' and now often referred to as the 'Maxwell–Weichert model' [10] can be applied both in structural dynamics and in rotordynamics. This model can be applied in both frequency domain and time domain formulations and leads to results that, at least in a given frequency range, are very close to those obtained using the hysteretic damping model.

A different approach was introduced by Bagley and Torvick [11,12]. It is based on a fractional derivative model and can model the damping of actual engineering materials in a wide frequency range with good precision.

The GHM (Golla, Hughes, McTavish) model [13,14] is based on the Maxwell–Weichert model but is formulated in such a way that it is suitable to be used in the context of the FEM (finite element method).

More recently, the term 'nonviscous damping' has been used for this kind of energy dissipation, mainly by Adhikari [15–20], who applied it to study in detail the behavior of damped vibrating systems of different types. The term *nonviscous damping* will be used throughout this paper. The aim of the present paper is to show that the nonviscous damping model can be easily applied to both hysteretic rotating and nonrotating damping in rotordynamics even in the context of the finite element modeling of complex rotors.

2. Simplified equivalent damping

2.1. Single-degree of freedom system

Consider a mass-spring–(viscous) damper system and a system with the same inertia and stiffness but with hysteretic damping with loss factor η. By comparing the equations of motion in the frequency domain, it is clear that the two systems are exactly equivalent if the damping coefficient of the former is related to the loss factor of the latter by the relationship

$$c_{\mathrm{eq}} = \frac{k\eta}{\omega} = \frac{k''}{\omega}. \tag{1}$$

Note that c_{eq}, usually referred to as the 'equivalent' damping coefficient, is necessarily a positive quantity (if it were negative, it would generate energy instead of dissipating it), and thus ω must be positive. As pointed out in [7], failure to recognize this fact resulted in many incorrect statements in the past.

However, the usefulness of Eq. (1) is dubious: the value of the equivalent damping coefficient depends on the frequency of vibration (to be more precise, to the frequency at which the material goes through its hysteresis cycle) and thus cannot be introduced into time domain equations. Moreover, the equivalent damping tends to infinity when the frequency tends to zero. This effect is discussed in detail in [3]. A common approximation is that of replacing the natural frequency of the system, which in a single degrees of freedom system gives

$$\omega_n = \sqrt{\frac{k}{m}}$$

for the generic frequency ω, obtaining

$$c_{\mathrm{eq}} = \frac{k\eta}{\omega_n} = \eta\sqrt{km}. \tag{2}$$

By introducing the damping ratio ζ, defined as the ratio between c and the critical damping $c_{\mathrm{cr}} = 2\sqrt{km}$, it follows that

$$\zeta_{\mathrm{eq}} = \frac{\eta}{2}. \tag{3}$$

The rationale behind this approximation is the consideration that when damping is small, it influences the response of the system only when it works close to its resonant frequency, and thus Eq. (2) yields a good approximation when damping is important. When it yields a poor approximation, damping has at any rate little effect on the behavior of the system.

2.2. Systems with many degrees of freedom

The conversion from hysteretic to equivalent viscous damping can be performed by resorting to modal decomposition. Consider a multi-degrees of freedom system with mixed viscous and hysteretic damping, whose frequency domain dynamic stiffness matrix is

$$\mathbf{K}_{\mathrm{dyn}} = -\omega^2\mathbf{M} + \mathrm{i}\omega\mathbf{C} + \mathbf{K} + \mathrm{i}\mathbf{K}''. \tag{4}$$

The eigenvector matrix $\mathbf{\Phi}$ of the corresponding MK system allows for computing the modal mass and stiffness matrices $\overline{\mathbf{M}}$ and $\overline{\mathbf{K}}$. In a similar way, an imaginary modal stiffness matrix can be obtained as

$$\overline{\mathbf{K}}'' = \mathbf{\Phi}^{\mathrm{T}}\mathbf{K}''\mathbf{\Phi}. \tag{5}$$

If either $\mathbf{K}'' = \eta\mathbf{K}$ or the usual relationships for generalized proportional damping hold, $\overline{\mathbf{K}}''$ is diagonal. If not, but the system is lightly damped as usually occurs for structural damping, it is possible to obtain the modal hysteretic damping for each mode by extracting the terms of $\overline{\mathbf{K}}''$ lying on the main diagonal. Applying Eq. (2), an equivalent viscous damping matrix

$$\overline{\mathbf{C}}_{\mathrm{eq}} = \mathrm{diag}\left(\frac{\overline{\mathbf{K}_{ii}}''}{\omega_{n_i}}\right) \tag{6}$$

is readily obtained and back-transformed

$$\mathbf{C}_{\mathrm{eq}} = \mathbf{\Phi}^{-1^{\mathrm{T}}}\overline{\mathbf{C}}_{\mathrm{eq}}\mathbf{\Phi}^{-1}. \tag{7}$$

Often it is not necessary to compute the equivalent damping of all modes but only that of the modes resonating in the frequency range of interest. In this case a reduced modal transformation, obtained through the reduced matrix of the eigenvectors $\mathbf{\Phi}^*$ can be used. Eq. (7) cannot be used directly in this case because $\mathbf{\Phi}^*$ is not square. The inverse transformation can, however, be performed by using the matrix

$$\overline{\mathbf{M}}^{-1}\mathbf{\Phi}^{\mathrm{T}}\mathbf{M}$$

instead of $\mathbf{\Phi}^{-1}$ [4]. The time-domain equation of motion is thus

$$\mathbf{M}\ddot{\mathbf{x}} + (\mathbf{C} + \mathbf{C}_{\mathrm{eq}})\dot{\mathbf{x}} + \mathbf{K}\mathbf{x} = \mathbf{F}(t). \tag{8}$$

Only hysteretic damping must be small: the viscous damping matrix $\mathbf{C}$ may be arbitrary large, and some (or even all) of the modes may be overdamped. Clearly, if all modes are overdamped and hysteretic damping is low, the latter may be neglected. The same procedure can be followed even in the case of nonlinear systems, provided that the viscoelastic elements are linear.

2.3. Rotating systems

It is well known that rotating hysteretic damping is stabilizing in subcritical conditions and destabilizing in supercritical ones [21,7] and also that, while viscous rotating damping causes a gradual decrease of stability with speed, in the case of hysteretic rotating damping the decrease is abrupt when crossing a relevant critical speed [1]. Consider a Jeffcott rotor with mass m and stiffness k, rotating at a spin speed Ω. Assume that both rotating and nonrotating damping are present and that the imaginary parts of the stiffness are k_r'' for the former and k_n'' for the latter. The Campbell diagram

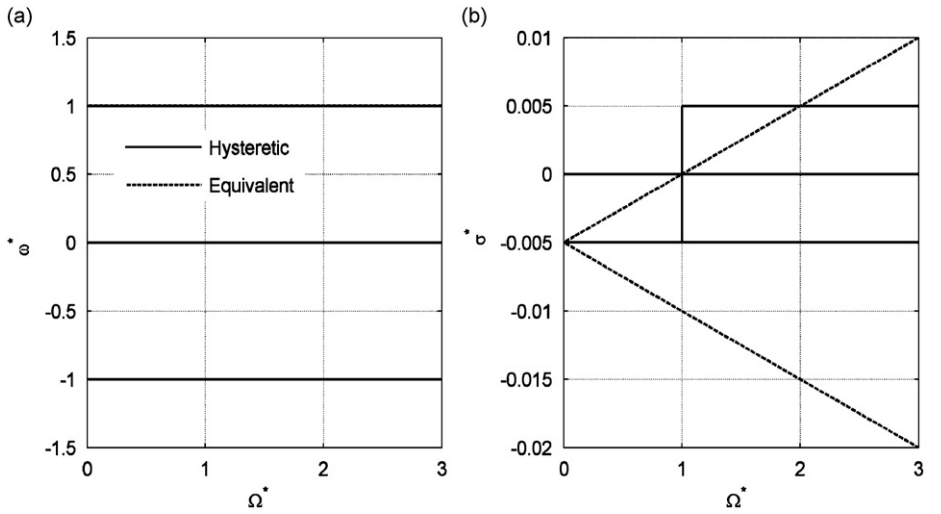

Fig. 1. Nondimensional Campbell diagram (a) and decay rate plot (b) for a hysteretically damped Jeffcott rotor with $k_n''=0$ and $k_n''/k=0.1$. The nondimensional whirl and spin speed and decay rate are $\omega^*=\omega\sqrt{m/k}$, $\Omega^*=\Omega\sqrt{m/k}$ and $\sigma^*=\sigma\sqrt{m/k}$.

and the decay rate plot for the case with $k_n''=0$ and $k_r''/k=0.01$ are reported in nondimensional form in Fig. 1. The Campbell diagram is flat, and the decay rate plot shows an abrupt increase of the decay rate of the forward mode when crossing the critical speed. This step causes instability ($R(s)>0$) because $k_n''<k_r''$: the threshold of instability coincides with the critical speed. In the case of a Jeffcott rotor, no threshold of instability would be present if $k_n''>k_r''$.

In the case of a general multi-degrees of freedom rotor, the decay rate plot would show multiple steps at the crossing of the various critical speeds, and the threshold of instability, if present, would coincide with one of them. These features are well known. If a time-domain computation, like that related to the 'blade-loss' problem or operation at variable speed (like a quick critical speed crossing), has to be performed, the hysteretic damping must be transformed into a form of damping allowing a time-domain formulation.

If the concept of simple equivalent damping seen above is used, the values of the equivalent damping coefficients are

$$c_{j_{eq}}=\frac{k_j''}{\omega_n}=k_j''\sqrt{\frac{m}{k}} \quad \text{for } j=n,r. \tag{9}$$

The results for the same case are shown in nondimensional form in Fig. 1 with dashed lines. The Campbell diagram is flat and approximates well the result obtained using the hysteretic damping model, but the decay rate plot is completely different. The branch for the backward mode decreases steadily, while that for the forward whirling increases without steps. The threshold of instability is the same in this case, but if the data were different it would have been different. In particular, if $k_n''>k_r''$ the system with hysteretic damping would have been stable at any speed, while that with equivalent viscous damping would have a threshold of instability at

$$\omega^*=1+\frac{k_n''}{k_r''}. \tag{10}$$

Similar results occur for multi-degrees of freedom rotors. The Campbell diagram and the decay rate plot for the rotor of a small turbine used as Example 24.2 in [4] with hysteretic and equivalent damping are compared in Fig. 2. The loss factor of the rotor is assumed to be $\eta_r=0.04$, while the two bearings are assumed to be hysteretically damped springs with k=20 MN/m and $\eta_n=0.06$. The model was reduced through Guyan reduction, obtaining a model with eight complex degrees of freedom. The computations were performed using the DYNROT code [22]. The transformation of hysteretic into equivalent damping was performed using the option 'Dyntrans' built in the code.

It is clear that the two models yield the same Campbell diagram, but the decay rate plots are quite different. In particular, as expected, the two forward branches, which have a critical speed in the range studied, show an abrupt decrease of the decay rate (in absolute value). In this case, the stability of the first forward mode is decreased when the equivalent model is used, while that of the second mode is increased. At vanishing speed, i.e., when the rotor reduces to a structure, the equivalent model yields correct results, which become increasingly inaccurate with increasing speed. The rotor with hysteretic damping is always stable, while that with equivalent viscous damping has a threshold of instability at about 38,000 rpm.

Two conclusions can be drawn from these examples:

- The viscous equivalent model seems adequate for the rotor at standstill. This confirms the observation in [23].
- When the rotor spins the equivalent viscous model remains adequate for computing the Campbell diagram (which is fairly obvious because it is well known that the natural frequencies are barely affected by damping, if the latter is small

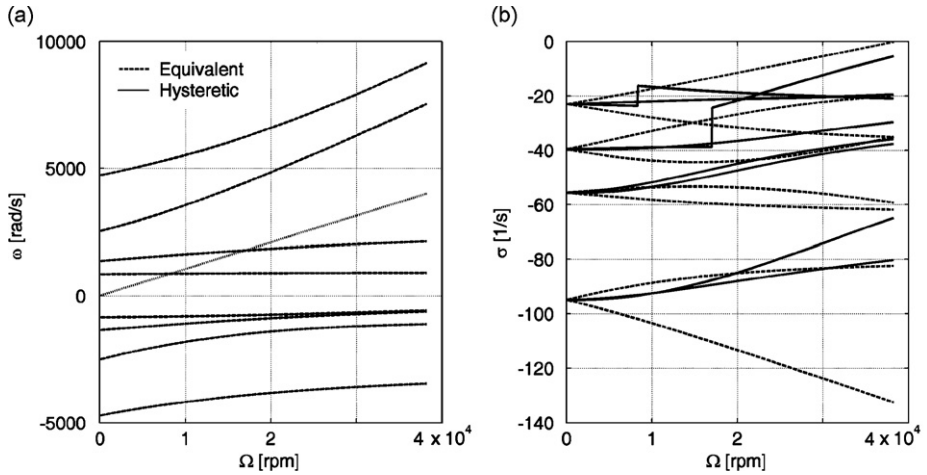

Fig. 2. Campbell diagram (a) and decay rate plot (b) for a multi-degrees of freedom rotor computed using the hysteretic and equivalent damping models.

enough) but not for the computation of the decay rate plot and above all for assessing the stability of the system at high speed.

A further observation is that the comparison is performed in a frequency domain computation because the hysteretic model applies only in this case. The rationale for this way of proceeding is that if the hysteretic damping model simulates the actual behavior of the system in harmonic motion properly, while the equivalent damping model is inadequate, the latter should not be used when the system performs a motion of another type.

3. Nonviscous damping

The conclusions drawn in the previous section suggest looking for a different approach for transforming the hysteretic damping in such a way that it can be used in the time domain computations. A general model for a material in which the stress is not only dependent on the instant values of the strain and strain rate (like in visco-elastic materials) but also on the past histories is

$$\sigma = E\left(\varepsilon - \int_{-\infty}^{t} G(t,\tau)\dot{\varepsilon}(\tau)\,\mathrm{d}\tau\right), \tag{11}$$

where function $\mathcal{G}(t,\tau)$, which usually has the form $\mathcal{G}(t-\tau)$, is referred to as the *damping kernel*, *retardation*, *heredity*, *after-effect* or *relaxation* function of the material [13–20]. This constitutive law accounts for both creep and relaxation.

A common expression for the damping kernel function is a sum of exponential terms

$$G(t-\tau) = \sum_{i=1}^{m} c_i \mu_i \mathrm{e}^{-\mu_i (t-\tau)}, \tag{12}$$

where the m parameters μ_i are called *relaxation parameters*. If all μ_i tend to infinity, viscous damping is obtained.

The equation of motion of a system with a single degree of freedom, which includes nonviscous damping as well, modeled using Eq. (11) together with Eq. (12) to express the damping kernel, is

$$m\ddot{x} + c\dot{x} + \sum_{i=1}^{m} c_i \mu_i \int_{-\infty}^{t} \mathrm{e}^{-\mu_i (t-\tau)} \dot{x}(\tau)\,\mathrm{d}\tau + kx = f(t). \tag{13}$$

It is possible to demonstrate that each exponential term in Eq. (12) yields a force equivalent to it due to a spring with a damper in series (the system in Fig. 3a). This model is thus equivalent to the Maxwell–Weichart model with a number m of spring–damper branches, each one with a damper c_i and a spring with stiffness $k_i = c_i \mu_i$.

It is also possible to show that if the number of branches tends to infinity this model coincides, in the frequency domain, with the hysteretic damping model [9,23]. Clearly, in any real world application the value of m must be limited (and possibly small), and thus the hysteretic model can be simulated only in a given frequency range. In [23], it was shown that this frequency range is about m decades wide, with a fairly flat imaginary part of the complex stiffness. In the same paper, some criteria are given for the choice of the values of μ_i that must be done according to the requirements that the frequency range is centered on the natural frequency of the system and is wide enough.

As clearly shown in Fig. 3a, a number m of degrees of freedom, corresponding to the displacements of points B_i, must also be considered. They are usually referred to as *internal* or *damping degrees of freedom*. A system with a single degree of freedom is thus transformed into a system with $m+1$ degree of freedom; while if the original system had n degrees of

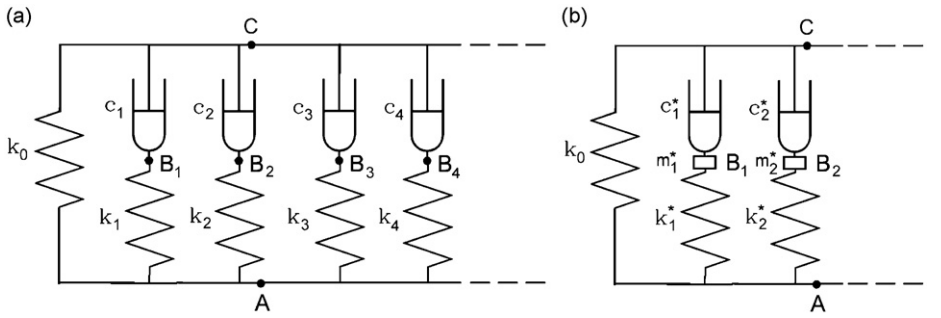

Fig. 3. (a) The nonviscous damping model. (b) A different version of the same model, as used in the GHM method.

freedom, the transformed system has $n(m+1)$ degrees of freedom. However, because no mass is associated with points B_i, the accelerations of the internal coordinates do not appear in the equations of motion, and the order of the resulting set of equations is not $2n(m+1)$ but only $n(m+2)$. When resorting to the state space approach, the state variables are thus $n(m+2)$. The equation of motion of the system with a single degree of freedom of Fig. 3a with mass m located in point C, possibly a viscous damper with coefficient c, and constrained in point A is

$$\mathbf{M}\ddot{\mathbf{x}}+\mathbf{C}\dot{\mathbf{x}}+\mathbf{K}\mathbf{x}=\mathbf{f}(t), \tag{14}$$

where, remembering Eq. (13), the relevant matrices and vectors are

$$\mathbf{x}=\begin{Bmatrix} x_C \\ x_{B1} \\ x_{B2} \\ \dots \end{Bmatrix}, \quad \mathbf{M}=\begin{bmatrix} m & 0 & 0 & \dots \\ & 0 & 0 & \dots \\ & & 0 & \dots \\ \text{symm.} & & & \dots \end{bmatrix}, \quad \mathbf{f}(t)=\begin{Bmatrix} F_c \\ 0 \\ 0 \\ 0 \end{Bmatrix},$$

$$\mathbf{C}=\begin{bmatrix} c+\sum_{i=1}^{m} c_i & -c_1 & -c_2 & \dots \\ & c_1 & 0 & \dots \\ & & c_2 & \dots \\ \text{symm.} & & & \dots \end{bmatrix}, \quad \mathbf{K}=\begin{bmatrix} k & 0 & 0 & \dots \\ & \mu_1 c_1 & 0 & \dots \\ & & \mu_2 c_2 & \dots \\ \text{symm.} & & & \dots \end{bmatrix}.$$

Because the states are only $m+2$, the state equation is

$$\begin{Bmatrix} \dot{v}_C \\ \dot{x}_C \\ \dot{\mathbf{x}}_B \end{Bmatrix}=\mathbf{M}^{*-1}\mathcal{A}^*\begin{Bmatrix} v_C \\ x_C \\ \mathbf{x}_B \end{Bmatrix}+\mathbf{M}^{*-1}\begin{Bmatrix} F_C \\ 0 \\ \mathbf{0}_{m\times 1} \end{Bmatrix}, \tag{15}$$

where

$$\mathbf{M}^*=\begin{bmatrix} m & 0 & \mathbf{C}_{12} \\ \mathbf{0}_{m\times 1} & \mathbf{0}_{m\times 1} & \mathbf{C}_{22} \\ 0 & 1 & \mathbf{0}_{1\times m} \end{bmatrix}, \quad \mathcal{A}^*=-\begin{bmatrix} C_{11} & K_{11} & \mathbf{0}_{1\times m} \\ \mathbf{C}_{21} & \mathbf{0}_{m\times 1} & \mathbf{K}_{22} \\ -1 & 0 & \mathbf{0}_{1\times m} \end{bmatrix}, \tag{16}$$

and the submatrices $\mathbf{C}_{ij}$ and $\mathbf{K}_{ij}$ of the damping and stiffness matrices are such that C_{11} and K_{11} are numbers, $\mathbf{C}_{12}$ is a row matrix with m columns and $\mathbf{C}_{22}$ and $\mathbf{K}_{22}$ are $m\times m$ diagonal matrices. This form of the state equations is not unique, and many different forms, all essentially equivalent, can be found in the literature (e.g. [17]). In the case of systems with many degrees of freedom, the coordinates x_C and x_{Bi} and the force F_c are substituted by vectors of order n and parameters m, c and k are matrices of order $n\times n$. Note that in a complex system the nonviscous damping parameters c_i and μ_i may be different in the various elements. It is then possible to use a larger number of nonviscous damping parameters, setting all elements in each matrix c_i and $\mu_i c_i$ equal to zero except for those of the material of the relevant element. These matrices are thus rank deficient, but this does not cause problems, except for the fact that, with the number of coefficients m larger, the size of all matrices is quite large as well.

It must be stated that the increase of the number of states of the system, while increasing the number of the poles and the corresponding number of modes, does not affect the number of modes with an oscillatory character. The added modes are all overdamped, and their poles are close to the real poles μ_i of the various spring–damper branches.

A different, although essentially equivalent, approach is followed by the GHM method: instead of introducing m spring–damper branches, a number $m/2$ of mass-spring–damper branches are added (Fig. 3b) [13,14]. In [14], they are referred to as *mini-oscillators*, but their free behavior is not oscillatory because they are overdamped. In this way, the mass matrix is not singular, and the usual way for building the state space dynamic matrix can be followed. Anyway, the total number of state variables is again $n(m+2)$.

4. The Jeffcott rotor with nonviscous damping

Consider the same Jeffcott rotor studied in Section 2.3, with both rotating and nonrotating hysteretic damping. Rotating and nonrotating damping must be taken into account separately: if each is modeled using m spring–damper systems, a total of $2m$ points B_j and then internal degrees of freedom, must be added. In the following, subscripts nj are used for the points located on the branches simulating nonrotating damping and rj for those in the rotating dampers. The complex-coordinate vector [11] is thus

$$\mathbf{q} = [r_A \;\; r_{B_{n1}} \;\; r_{B_{r1}} \;\; r_{B_{n2}} \;\; r_{B_{r2}} \;\; \cdots \;\; r_{B_{nn}} \;\; r_{B_{rn}}]^{\mathrm{T}}. \tag{17}$$

The time-domain equation of motion is

$$m\mathbf{M}^*\ddot{\mathbf{q}} + \sqrt{km}(\mathbf{C}_n^* + \mathbf{C}_r^*)\dot{\mathbf{q}} + (k\mathbf{K}^* - j\Omega\sqrt{km}\mathbf{C}_r^*)\mathbf{q} = [m\Omega^2 \mathrm{e}^{\mathrm{i}\Omega t} + f_n(t)]\mathbf{F}^*, \tag{18}$$

where the nondimensional mass, stiffness and damping matrices are

$$\mathbf{M}^* = \mathrm{diag}[1 \;\; 0 \;\; 0 \;\; \ldots \;\; 0], \tag{19}$$

$$\mathbf{K}^* = \begin{bmatrix} 1+\eta_n\sum_{\forall j}\gamma_{nj}+\eta_r\sum_{\forall j}\gamma_{rj} & -\eta_n\gamma_{n1} & -\eta_r\gamma_{r1} & \cdots & -\eta_r\gamma_{rn} \\ & \eta_n\gamma_{n1} & 0 & \cdots & 0 \\ & & \eta_r\gamma_{r1} & \cdots & 0 \\ & & & \cdots & 0 \\ & \text{symm.} & & & \eta_r\gamma_{rn} \end{bmatrix}, \tag{20}$$

$$\mathbf{C}_n^* = \eta_n \mathrm{diag}\left[0 \;\; \frac{\gamma_{n1}}{d_{n1}} \;\; 0 \;\; \frac{\gamma_{n2}}{d_{n2}} \;\; 0 \;\; \ldots \;\; \frac{\gamma_{nn}}{d_{nn}} \;\; 0\right], \tag{21}$$

$$\mathbf{C}_r^* = \eta_r \mathrm{diag}\left[0 \;\; 0 \;\; \frac{\gamma_{r1}}{d_{r1}} \;\; 0 \;\; \frac{\gamma_{r2}}{d_{r2}} \;\; \ldots \;\; 0 \;\; \frac{\gamma_{rn}}{d_{rn}}\right], \tag{22}$$

and

$$\eta_n = \frac{k_n''}{k}, \quad \eta_r = \frac{k_r''}{k}, \quad d_j = a^{(2j-n-1)/2}. \tag{23}$$

Vector $\mathbf{F}^*$ is

$$\mathbf{F}^* = [1 \;\; 0 \;\; 0 \;\; \ldots \;\; 0]^{\mathrm{T}}. \tag{24}$$

Because the mass matrix $\mathbf{M}^*$ is singular, a reduced complex state vector must be introduced

$$\mathbf{z} = [v \;\; \mathbf{r}^{\mathrm{T}}]^{\mathrm{T}} = [v \;\; r_A \;\; r_{B_{n1}} \;\; r_{B_{r1}} \;\; r_{B_{n2}} \;\; \ldots \;\; r_{B_{rn}}]^{\mathrm{T}}, \tag{25}$$

where $v = \dot{r}_A$. By partitioning all matrices into four submatrices, in such a way to keep the first degree of freedom, with which a finite mass is associated, separated from the others, the dynamic matrix of the system can be shown to be

$$\mathbf{A}^* = -\begin{bmatrix} 1 & 0 & \mathbf{0} \\ \mathbf{0} & \mathbf{0} & (\mathbf{C}_{n22}^* + \mathbf{C}_{n22}^*) \\ 0 & 1 & \mathbf{0} \end{bmatrix}^{-1} \begin{bmatrix} 0 & K_{11}^* & \mathbf{K}_{12}^* \\ 0 & \mathbf{K}_{21}^* & \mathbf{K}_{22}^* - i\Omega^*\mathbf{C}_{r22}^* \\ -1 & 0 & \mathbf{0} \end{bmatrix}, \tag{26}$$

where the nondimensional spin speed Ω^* is

$$\Omega^* = \Omega\sqrt{\frac{m}{k}}.$$

Eq. (26) is justified by remembering that $M_{11}^* = 1$ and that C_{r11}^* (a number), $\mathbf{M}_{12}^*$ and $\mathbf{C}_{r12}^*$ (row matrices), $\mathbf{M}_{21}^*$ and $\mathbf{C}_{r21}^*$ (column matrices) and $\mathbf{M}_{r22}^*$ and $\mathbf{C}_{r22}^*$ (square matrices), all vanish. The same is true for the matrices of nonrotating damping.

The eigenvalues of the dynamic matrix $\mathbf{A}^*$ are the nondimensional roots of the system: their imaginary parts are now the nondimensional whirl frequencies, and their real parts the nondimensional decay rates. In the case of a single damper, $\gamma_{n1} = \gamma_{r1} = 2$ and the dynamic matrix is reduced to

$$\mathbf{A}^* = \begin{bmatrix} 0 & -1-2\eta_n-2\eta_r & 2\eta_n & -2\eta_r \\ 1 & 0 & 0 & 0 \\ 0 & 1 & -1 & 0 \\ 0 & 1 & 0 & -1+\mathrm{i}\Omega^* \end{bmatrix}.$$

The nondimensional Campbell diagram and decay rate plot of the same Jeffcott rotor studied in Section 3 (Fig. 1) are reported in Fig. 4. The solution for hysteretic damping is compared with that for a nonviscous damper with m=1, 2 and 3. While in the hysteretic damping case there are only two solutions, one for forward and one for backward whirling, by adding m degrees of freedom, a further m solutions are found (only m and not $2m$ because the added states are only m). The

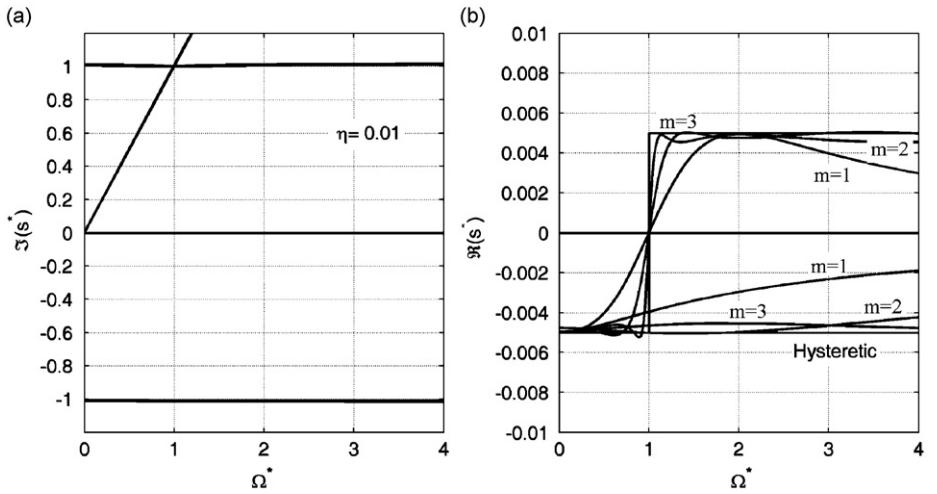

Fig. 4. Nondimensional Campbell diagram (a) and decay rate plot (b) for a Jeffcott rotor with hysteretic rotating damping with loss factor $\eta = 0.01$. The solution for hysteretic damping is compared with that for a nonviscous damper with m=1, 2 and 3.

added solutions are, however, synchronous and stable whirling motions with a high decay rate and are therefore of little interest. They correspond to the nonoscillatory solutions of the vibrating system with NVD [14], and they are actually nonoscillatory in the rotating plane. The Campbell diagram is thus essentially the same as that for hysteretic damping, while in the decay rate the abrupt step typical of hysteretic damping is replaced with a more gradual passage from subcritical stability to supercritical instability of forward whirling. By increasing the number of dampers the passage is more abrupt, and with m=3 the step is almost restored.

If n=4 and $\Omega^* = 0$, the values of s^* are $-0.0044 \pm 1.0152i$ (the poles of the original system), plus -31.6222, -3.1584, -0.3124, -0.0311. The absolute values of the latter four are very close to the four values of β_i.

When $\Omega^* = 4$, the values are $-0.0048-1.0202$i for the backward whirl, 0.0049+1.0183i for the forward (unstable) whirl, and then $-31.6223+4.0001$i, $-3.1626+4.0016$i, $-0.3165+4.0000$i, $-0.0317+4.0000$i for the additional modes due to the internal degrees of freedom. As already stated, they are practically synchronous whirling motion, i.e., nonoscillatory motions in the rotating frame. There are only four because only rotating damping was considered.

5. Rotors with many degrees of freedom

Consider a multi-degrees of freedom rotor, with both viscous and hysteretic damping. Neglecting hysteretic damping, under the assumption of axial symmetry of both the rotor and the stator of the machine, the time-domain equation of motion, written in complex coordinates [1], is

$$\mathbf{M}\ddot{\mathbf{q}} + (\mathrm{i}\Omega\mathbf{G} + \mathbf{C}_n + \mathbf{C}_r)\dot{\mathbf{q}} + (\mathbf{K} - \mathrm{i}\Omega\mathbf{C}_r)\mathbf{q} = \mathbf{F}(\mathbf{t}), \tag{27}$$

where the gyroscopic matrix $\mathbf{G}$ is symmetric because complex coordinates are used. The eigenvector matrix $\mathbf{\Phi}$ of the corresponding MK system allows for the computation of the modal matrices, in this case including also the modal gyroscopic matrix $\overline{\mathbf{G}}$, which is in general nondiagonal. After performing the modal transformation, two nonviscous dampers, a rotating and a nonrotating one, can be added to each modal system to simulate both rotating and nonrotating damping. By doing so, a number $2m$ of internal degrees of freedom must be added for each mode considered, if m is the number of branches of each one of the nonviscous dampers. Note that not all modal systems need to be damped, and that it is not necessary to add the same number of dampers to all modes.

By partitioning the matrices in the same way seen for the Jeffcott rotor, and remembering that several submatrices vanish, the modal equation of motion is thus

$$\begin{bmatrix} \overline{\mathbf{M}} & \mathbf{0} \\ \mathbf{0} & \mathbf{0} \end{bmatrix} \begin{Bmatrix} \ddot{\boldsymbol{\eta}} \\ \ddot{\mathbf{x}}_B \end{Bmatrix} + \begin{bmatrix} -\mathrm{i}\Omega\overline{\mathbf{G}} + \overline{\mathbf{C}}_n + \overline{\mathbf{C}}_r & \mathbf{0} \\ \mathbf{0} & \mathbf{C}_{r22} + \mathbf{C}_{n22} \end{bmatrix} \begin{Bmatrix} \dot{\boldsymbol{\eta}} \\ \dot{\mathbf{x}}_B \end{Bmatrix} + \begin{bmatrix} \overline{\mathbf{K}} + \mathbf{K}_{11} - \mathrm{i}\Omega\overline{\mathbf{C}}_r & \mathbf{K}_{12} \\ \mathbf{K}_{21} & \mathbf{K}_{22} - \mathrm{i}\Omega\mathbf{C}_{r22} \end{bmatrix} \begin{Bmatrix} \boldsymbol{\eta} \\ \mathbf{x}_B \end{Bmatrix} = \begin{Bmatrix} \overline{\mathbf{F}} \\ \mathbf{0} \end{Bmatrix}, \tag{28}$$

where to the modal complex coordinates $\boldsymbol{\eta}$ another set of complex coordinates $\mathbf{x}_B$ has been added. The overlined matrices are the modal matrices of the system with viscous damping, while the nonoverlined ones are the matrices added to simulate hysteretic damping. Generally speaking $\overline{\mathbf{G}}$, $\overline{\mathbf{C}}_n$ and $\overline{\mathbf{C}}_r$ are not diagonal. For each mode considered (the rth mode is

considered in the formulas), matrices **C** and **K** have a structure of the kind

$$\mathbf{K}=\overline{\overline{\mathbf{K}}}_{n_{rr}}\begin{bmatrix}\sum_{\forall j}\gamma_{nj} & -\gamma_{n1} & 0 & \dots & 0\\ & \gamma_{n1} & 0 & \dots & 0\\ & & 0 & \dots & 0\\ & & & \dots & 0\\ \text{symm.} & & & & 0\end{bmatrix}+\overline{\overline{\mathbf{K}}}_{r_{rr}}\begin{bmatrix}\sum_{\forall j}\gamma_{ri} & 0 & -\gamma_{r1} & \dots & -\gamma_{rn}\\ & 0 & 0 & \dots & 0\\ & & \gamma_{r1} & \dots & 0\\ & & & \dots & 0\\ \text{symm.} & & & & \gamma_{rn}\end{bmatrix}, \tag{29}$$

$$\mathbf{C}_n=\overline{\overline{\mathbf{K}}}_{n_{rr}}\mathrm{diag}[0\ \ \gamma_{n1}/\mathrm{d}_{n1}\ \ 0\ \ \dots\ \ 0], \tag{30}$$

$$\mathbf{C}_r=\overline{\overline{\mathbf{K}}}_{r_{rr}}\mathrm{diag}[0\ \ 0\ \ \gamma_{r1}/d_{r1}\ \ \dots\ \ \gamma_{rn}/d_{rn}]. \tag{31}$$

As already stated, out of the four submatrices of each damping matrix, only $\mathbf{C}_{22}$ does not vanish. If a solution in the original coordinates (plus obviously coordinates $\mathbf{x}_B$) is required, it is possible to resort to the obvious equation

$$\begin{Bmatrix}\mathbf{x}\\ \mathbf{x}_B\end{Bmatrix}=\begin{bmatrix}\boldsymbol{\Phi} & \mathbf{0}\\ \mathbf{0} & \mathbf{I}\end{bmatrix}\begin{Bmatrix}\boldsymbol{\eta}\\ \mathbf{x}_B\end{Bmatrix}$$

to back-transform the matrices.

Note that the back-transformation is still possible even if a reduced number of modes has been considered, and hence the reduced matrix of the eigenvectors $\boldsymbol{\Phi}^*$ is not square. In this case

$$\begin{Bmatrix}\boldsymbol{\eta}\\ \mathbf{x}_B\end{Bmatrix}=\begin{bmatrix}\overline{\mathbf{M}}^{-1}\boldsymbol{\Phi}^{\mathrm{T}}\mathbf{M} & \mathbf{0}\\ \mathbf{0} & \mathbf{I}\end{bmatrix}\begin{Bmatrix}\mathbf{x}\\ \mathbf{x}_B\end{Bmatrix}.$$

No errors due to gyroscopic effects and large viscous damping are introduced if all modes are used, so that the procedure can be used for overdamped systems or strongly gyroscopic ones as well. What is required is only that the hysteretic component of damping is small.

However, it is possible to use a limited number of modes and then to back-transform the equivalent damping matrices to perform the relevant computation with reference to the physical complex coordinates **q**, suitably augmented with the complex coordinates $\mathbf{x}_B$. In this mode, the gyroscopic and viscous damping matrices need not be transformed into modal coordinates. To reduce the number of coordinates, the high frequency modes can be modeled using a smaller number of points B, and the same can be said for nonrotating damping.

6. Examples

6.1. Example 1: rotating beam on elastic supports

Consider a beam with an annular cross section (inner and outer diameters 60 and 50 mm) with a length of 1.5 m, constrained at the ends by two elastic supports with a stiffness of 2 MN/m. The beam is made from steel (E=211 GPa, $\rho=7810\,\mathrm{kg/m^3}$, $\nu=0.3$). The material of the beam has a loss factor $\eta_r=0.02$, while the elastic supports have a loss factor $\eta_n=0.06$. A nonrotating beam with slightly different supports was studied in [23]. By modeling the beam with 3 Timoshenko beam elements and eliminating the rotational degrees of freedom through a Guyan reduction, a system with only four degrees of freedom is obtained. The natural frequencies of the nonrotating beam are

$$\omega_n=\begin{cases}370.2\,\mathrm{rad/s}=58.92\,\mathrm{Hz},\\ 979.6\,\mathrm{rad/s}=155.91\,\mathrm{Hz},\\ 1718.6\,\mathrm{rad/s}=273.53\,\mathrm{Hz},\\ 3029.8\,\mathrm{rad/s}=482.21\,\mathrm{Hz}.\end{cases}$$

The damped poles of the nonrotating system with hysteretic damping are

$$s=\begin{cases}-6.0\pm370.3\mathrm{i}\,\mathrm{rad/s},\\ -25.2\pm980.1\mathrm{i}\,\mathrm{rad/s},\\ -40.7\pm1719.1\mathrm{i}\,\mathrm{rad/s},\\ -43.1\pm3030.1\mathrm{i}\,\mathrm{rad/s}.\end{cases}$$

By using the ‘equivalent damping’ approach the poles are

$$s=\begin{cases}-6.0\pm370.2\mathrm{i}\,\mathrm{rad/s},\\ -25.3\pm979.3\mathrm{i}\,\mathrm{rad/s},\\ -40.7\pm1718.1\mathrm{irad/s},\\ -43.1\pm3029.5\mathrm{i}\,\mathrm{rad/s}.\end{cases}$$

If a nonviscous damper with m=3 is added to each modal system, the system has a total of 28 degrees of freedom. However, there are only 32 states, and the poles are

$$s_{1,\dots,8} = \begin{cases} -6.0 \pm 378.5\mathrm{i}\ \mathrm{rad/s}, \\ -25.2 \pm 999.7\mathrm{i}\ \mathrm{rad/s}, \\ -40.6 \pm 1754.6\mathrm{irad/s}, \\ -42.5 \pm 3098.7\mathrm{i}\ \mathrm{rad/s}, \end{cases} \quad s_{9,\dots,12} = \begin{cases} -35.02\ \mathrm{rad/s}, \\ -37.02\ \mathrm{rad/s}, \\ -89.41\ \mathrm{rad/s}, \\ -97.96\ \mathrm{rad/s}, \end{cases}$$

$$s_{13,\dots,16} = \begin{cases} -158.13\ \mathrm{rad/s}, \\ -171.86\ \mathrm{rad/s}, \\ -288.74\ \mathrm{rad/s}, \\ -302.98\ \mathrm{rad/s}, \end{cases} \quad s_{17,\dots,20} = \begin{cases} -362.32\ \mathrm{rad/s}, \\ -370.22\ \mathrm{rad/s}, \\ -946.28\ \mathrm{rad/s}, \\ -979.62\ \mathrm{rad/s}, \end{cases}$$

$$s_{21,\dots,24} = \begin{cases} -1664.95\ \mathrm{rad/s}, \\ -1718.62\ \mathrm{rad/s}, \\ -2973.47\ \mathrm{rad/s}, \\ -3029.80\ \mathrm{rad/s}, \end{cases} \quad s_{25,\dots,28} = \begin{cases} -3700.19\ \mathrm{rad/s}, \\ -3702.22\ \mathrm{rad/s}, \\ -9787.68\ \mathrm{rad/s}, \\ -9796.20\ \mathrm{rad/s}, \end{cases}$$

$$s_{29,\dots,32} = \begin{cases} -17172.50\ \mathrm{rad/s}, \\ -17186.24\ \mathrm{rad/s}, \\ -30283.49\ \mathrm{rad/s}, \\ -30298.02\ \mathrm{rad/s}. \end{cases}$$

The first eight poles are complex and are essentially the same seen above except for a slight increase of the frequency due to the added stiffness. The remaining 24 are real as well as negative and correspond to much damped nonoscillatory modes that have practically no importance.

The Campbell diagram is little influenced by damping and, due to the negligible gyroscopic effect, is almost completely flat. It is not reported here. The decay rate plot is reported in Fig. 5. The lines labeled (H) describe the behavior of the system with hysteretic damping. At the critical speed, the decay rate of the first forward mode has an abrupt increase. It, however, remains negative, and the rotor is stable at all speeds. The lines labeled (E) are related to the simplified equivalent damping. The behavior is that typical of viscous damping: a gradual increase (decrease in absolute value) of the decay rate in forward whirling with a threshold of instability in the supercritical regime. While at standstill, the equivalent viscous damping is actually equivalent; when the system rotates the two forms of damping yield quite different results. This behavior is true not only in synchronous whirling, where the applicability of hysteretic damping is questionable because the frequency $\omega-\Omega$ of the hysteresis cycle vanishes, but at all speeds. In particular, at high speeds, the two solutions diverge. The equivalent model leads to a finite value of the threshold of instability, contrary to what happens with the hysteretic model. The curves labeled as (NV) were obtained by applying eight nonviscous dampers (four rotating and four nonrotating) to the four modal systems. Each of them has three spring–damper branches, tuned at the modal frequency and at frequencies 1/10 and 10 times the modal frequency. The total number of complex states of the system is

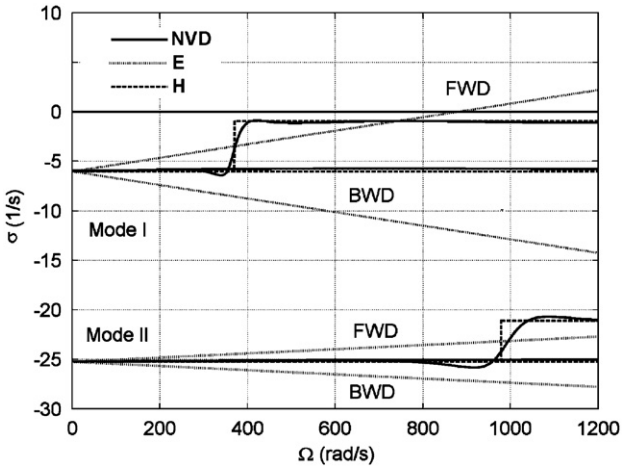

Fig. 5. Decay rate plot for the rotor described in example 1. The curves for hysteretic (H), equivalent (E) and nonviscous damping (NVD) are reported.

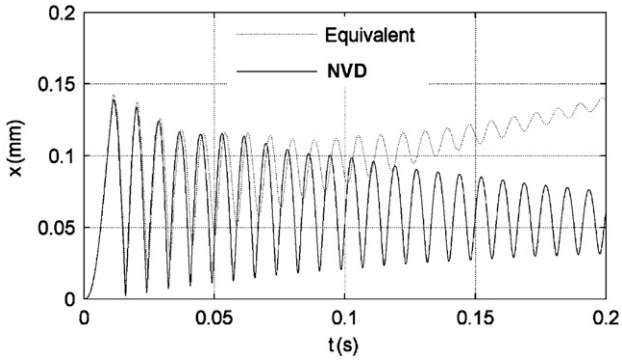

Fig. 6. Response of the rotor of Fig. 7 to a shock. Comparison between equivalent and nonviscous damping.

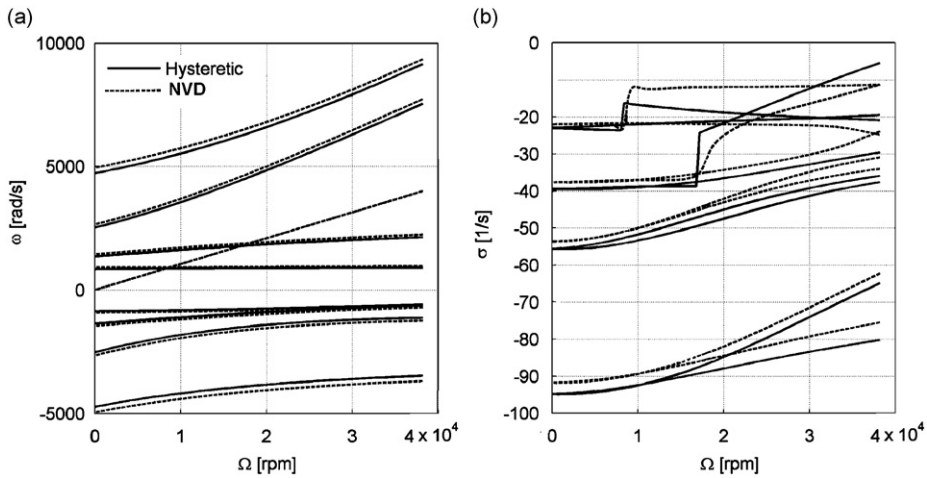

Fig. 7. Same as Fig. 2 but for hysteretic and nonviscous damping.

32 instead of 8. The behavior is much more similar to that related to hysteretic damping. The step of the decay rate is present, although less abrupt, and the threshold of instability is not present.

A shock-like excitation due to a nonrotating force growing linearly to 10,000 N in 11 ms is applied to a point at 500 mm from one end when the shaft rotates at 1400 rad/s. The response to the shock must be computed through numerical integration in time of the equations of motion. The results, in terms of the time history of the amplitude of the displacement in the rotation plane of the point where the shock is given, are plotted in Fig. 6. In case of nonviscous damping, the shock triggers a circular synchronous whirl, which stabilizes in time to a constant amplitude and then slowly decreases asymptotically to zero (this behavior is not shown in the figure because it takes several seconds). The oscillation slowly dampens out as well. In the case of the equivalent damping, because the rotor operates above its threshold of instability, the synchronous whirling grows without bounds, while the oscillations die out in a short time.

6.2. *Example 2: rotor with nonnegligible gyroscopic effect*

Consider the same multi-degrees of freedom rotor studied in Section 3 (Fig. 2). The results obtained using the NVD model are shown in Fig. 7. Three rotating and three nonrotating nonviscous dampers have been added for each mode. Because four modes were considered, the number of internal degrees of freedom or states of the system is 24, which must be added to the four degrees of freedom if the computation is performed in modal coordinates, for a total of 32 states. If the equations are back-transformed, there are eight degrees of freedom for the original system, for a total of 40 states. The computation was performed using both modal and nonmodal coordinates, obtaining exactly the same results for the four forward and four backward modes shown in the plot.

The nonviscous damper model has almost the same Campbell diagram as the one obtained using hysteretic damping. The small differences are due to the fact that the former model adds also some stiffness to the system and hence slightly modifies the natural frequencies. The decay rate is much closer to the one for hysteretic damping. In particular, it is characterized by abrupt decreases of the decay rate of the first two modes when they cross the relevant critical speeds.

Although not being exactly equal to the plot obtained for the hysteretic damping model, it at least corrects the largest errors introduced by the conventional equivalent damping model, in particular at high speed.

7. Conclusions

The nonviscous damping model, with a finite number of viscous dampers, allows for writing equations of motion in the time domain starting from the hysteretic damping formulation. It approximates the hysteretic behavior over a wide frequency range well, at the cost of a number of additional (usually referred to as internal or hidden) degrees of freedom.

Obviously it is impossible to compare the results of this model with those obtained through the hysteretic model in conditions other than harmonic motion because the latter cannot be used. However, when the system performs harmonic motions the two models yield reasonably close results.

One limitation is that hysteretic damping must be small, particularly when the system has many degrees of freedom, and the nonviscous dampers are applied to decouple the modal systems. However, it is possible to perform the modal transformation only where the hysteretic damping is concerned, and, if there are other forms of damping, they can be added later, after back-transforming the model to the 'physical coordinates' plus the internal ones. In this way, no small damping assumptions are required for the other forms of damping.

The other limitation of hysteretic damping, linked with its poor performance at low frequency, is circumvented. In this sense, the nonviscous damping model is better than the original hysteretic damping model when the system performs low frequency motions.

The nonviscous damping model is generalized here for rotordynamics. When dealing with rotating machinery the rotating damping must be dealt with separately from nonrotating damping, and thus the introduction of a larger number of internal degrees of freedom is required: for each mode, the number of spring–damper branches, and thus the number of internal degrees of freedom, is doubled if the rotating and nonrotating modal damping are modeled in the same way. This problem can be mitigated by using a smaller number of internal degrees of freedom for nonrotating damping because the problems linked with hysteretic damping are more serious in the case of rotating damping.

While the inconsistency of hysteretic damping in low frequency motion may be marginally important in structural dynamics, it constitutes a serious drawback in rotordynamics. In situations in which the whirl frequency is close to the spin speed (almost-synchronous whirling), the frequency of the hysteresis cycle is close to zero, which leads to a questionable applicability of the hysteretic damping concept. The fact that hysteretic rotating damping may cause a threshold of instability equal to one of the critical speeds is due to this problem and may be regarded as an oversimplification linked with the type of model.

For rotating damping, the nonviscous damping model is thus actually better than the original model even in harmonic motion, apart from being needed when solving time-domain equations like those encountered in nonsteady-state motion, for instance when accelerating through a critical speed or in the 'blade-loss' problem.

The present model behaves better than the usual constant equivalent damping model not only at the critical speed crossing but also at high speed. In particular, it retains the property of hysteretic damping of either locating the threshold of instability close to a critical speed or granting stability at all speeds, while viscous damping always causes instability at a speed large enough (even if in many cases this occurs at a speed well in excess of the actual one).

It is well known that the prediction of high speed stability of rotors is still problematic mostly due to the uncertainties about how to model damping. The present model offers a theoretical alternative to the simpler viscous damping model. Only experimentation will validate the results obtained through the two approaches.

Acknowledgments

The authors are grateful to one of the reviewers of the previous version of this manuscript for the suggestions and comments that led to an improved version of the manuscript.

References

[1] G. Genta, *Dynamics of Rotating Systems*, Springer, New York, 2005.
[2] N.O. Myklestadt, The concept of complex damping, *Journal of Applied Mechanics* 19 (1952) 284–286.
[3] S.H. Crandall, The role of damping in vibration theory, *Journal of Sound and Vibration* 11 (1) (1970) 3–18.
[4] G. Genta, *Vibration Dynamics and Control*, Springer, New York, 2008.
[5] S.H. Crandall, Rotordynamics, in: W. Kliemann, N. Sri Namachchivaya (Eds.), *Nonlinear Dynamics and Stochastic Mechanics*, CRC Press, Boca Raton, 1995.
[6] G. Ramanujam, C.W. Bert, Whirling and stability of flywheel systems, part 1: derivation of combined and lumped parameter models part II: comparison of numerical results obtained with combined and lumped parameter models, *Journal of Sound and Vibration* 88 (3) (1983) 369–420.
[7] G. Genta, On a Persisting misunderstanding on the role of hysteretic damping in rotordynamics, *Journal of Vibration and Acoustics* 126 (2004) 469–471.
[8] M.A. Biot, Linear thermodynamics and the mechanics of solids, *Proceedings of the 4th US National Congress on Applied Mechanics*, 1962.
[9] T.K. Caughey, Vibration of dynamic systems with linear hysteretic damping, linear theory.
[10] D. Roylance, *Engineering Viscoelasticity*, MIT, Cambridge, 2001.

[11] R.L. Bagley, B.J. Torvik, Fractional calculus—a different approach to finite element analysis of viscoelastic damped structures, *AIAA Journal* 21 (5) (1983) 741–748.
[12] R.L. Bagley, B.J. Torvik, Fractional calculus in the transient analysis of viscoelastic damped structures, *Proceedings of the AIAA/ASME/ASCE/AHS 24th Structures, Structural Dynamics and Material Conference*, Lake Tahoe, Nev, May 2–4, 1983.
[13] D.F. Golla, P.C. Hughes, Dynamics of viscoelastic structures—a time domain finite element formulation, *Journal of Applied Mechanics* 52 (1985) 897–906.
[14] D.J. McTavish, P.C. Hughes, Modeling of linear viscoelastic space structures, *Journal of Vibration and Acoustics* 115 (1993) 103–110.
[15] S. Adhikari, Eigenrelations for non-viscously damped systems, *AIAA Journal* 39 (2001) 1624–1630.
[16] S. Adhikari, Dynamics of non-viscously damped linear systems, *Journal of Engineering Mechanics* 128 (2002) 328–339.
[17] N. Wagner, S. Adhikari, Symmetric state-space formulation for a class of non-viscously damped systems, *AIAA Journal* 41 (2003) 951–956.
[18] S. Adhikari, N. Wagner, Analysis of asymmetric non-viscously damped linear dynamic systems, *Journal of Applied Mechanics* 70 (2003) 885–893.
[19] S. Adhikari, Qualitative dynamic characteristics of a non-viscously damped oscillator, *Proceedings of the Royal Society of London Series A* 461 (2005) 2269–2288.
[20] S. Adhikari, Dynamic response characteristics of a non-viscously damped oscillator, *Journal of Applied Mechanics* 75 (2008) 011003:1–12.
[21] M. Dimentberg, *Flexural Vibrations of Rotating Shafts*, Butterworth, London, England, 1961.
[22] G. Genta, D. Bassani, C. Delprete, DYNROT: a finite element code for rotordynamic analysis based on complex co-ordinates, *Engineering Computations* 13 (6) (1996) 86–109.
[23] G. Genta, N. Amati, *On the Equivalent Viscous Damping for Systems with Hysteresis*, Atti dell'Accademia delle Scienze di Torino, 2009.